

Adversarial Robustness for Unified Multi-Modal Encoders via Efficient Calibration

Chih-Ting Liao¹ Bin Ren^{3,4} Guofeng Mei⁵ Xu Zheng^{2*}

¹Mill Research AI ²HKUST(GZ)

³University of Pisa ⁴University of Trento ⁵Fondazione Bruno Kessler, Italy

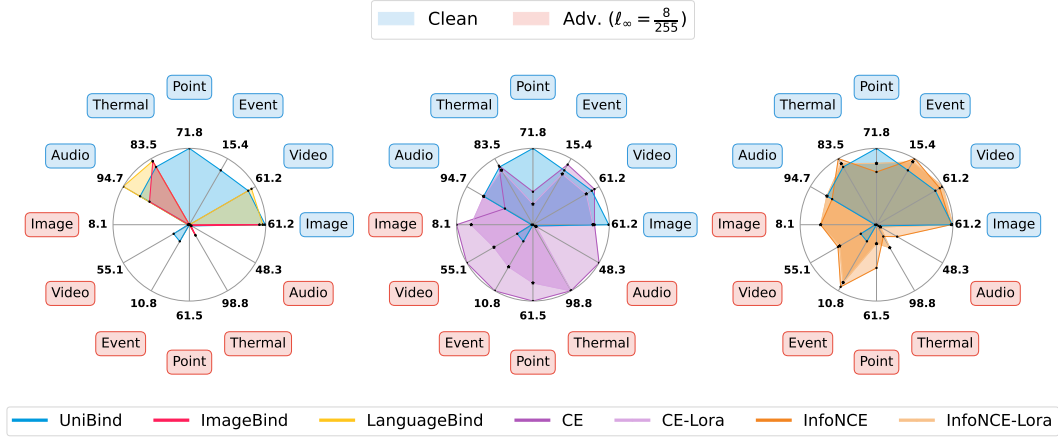


Figure 1: Radar charts showing clean and adversarial accuracy ($\ell_\infty = 8/255$) across six modalities: Image, Video, Event, Point, Thermal, and Audio. From left to right: (1) Three foundation models—UniBind, ImageBind, and LanguageBind; (2) UniBind, CE, and CE+LoRA; (3) UniBind, InfoNCE, and InfoNCE+LoRA. Blue areas represent clean accuracy, while red areas indicate adversarial performance under $\ell_\infty = 8/255$ perturbation. For full visualization, see Appendix Figure 4.

Abstract

Recent unified multi-modal encoders align a wide range of modalities into a shared representation space, enabling downstream cross-modal tasks. Despite impressive capabilities, the robustness of these models under adversarial perturbations remains unexplored—a critical concern for safety-sensitive applications. In this work, we conduct the *first* comprehensive study of adversarial vulnerability in unified multi-modal encoders. Under mild adversarial perturbations, these models experience substantial performance drops across all modalities. Non-visual inputs—such as audio and point cloud—are especially vulnerable, often failing entirely, while even visual modalities like image and video see significant declines. To address this, we propose an efficient adversarial calibration framework that improves robustness across modalities while keeping pretrained encoders and semantic centers frozen. This design ensures compatibility with existing foundation models and preserves alignment across the embedding space. Specifically, we introduce modality-specific projection heads trained solely on adversarial examples, maintaining frozen backbones and embeddings. We explore three objective functions—fixed-center cross-entropy, clean-to-adversarial L_2 alignment, and clean-adversarial InfoNCE—and further introduce a regularization strategy to ensure modality-consistent alignment under attack. Extensive experiments across six modalities and three Bind-style

*Corresponding Author: Xu Zheng <zhengxu128@gmail.com>

models demonstrate that our approach improves adversarial robustness by up to **+47.3%** at $\epsilon = 4/255$, while preserving or even improving clean zero-shot and retrieval performance with less than **1%** trainable parameters.

1 Introduction

Modern artificial intelligence (AI) systems are increasingly expected to perceive and reason across diverse sensory modalities—such as images, audio, text, video, depth, and thermal—mimicking human-like understanding of the world [1–20]. Multi-modal representation learning has emerged as a core strategy to support this capability, projecting heterogeneous inputs into a shared semantic space [1, 4, 21–23]. This allows machines to associate, for example, barking sounds with dog images, retrieve videos using text prompts, and generalize to new tasks via cross-modal transfer. Recent Bind-style models (*e.g.*, ImageBind, UniBind) achieve remarkable results in aligning modalities. However, they largely assume clean input conditions, overlooking robustness to noise, distribution shifts, and adversarial attacks. In real-world applications such as autonomous driving, robotics, and healthcare, such robustness is crucial [24–28]. Vulnerabilities in the shared embedding space—particularly for non-visual modalities—can lead to failure cascades in downstream tasks.

In vision-language settings, the robustness of CLIP [29] has been studied extensively. Prior work reveals its susceptibility to distribution shifts [30, 31] and adversarial examples [32], motivating robust training methods such as TeCo [33], TeCoA [32], and RobustCLIP [34]. However, these approaches are tailored to image-text models and cannot be directly applied to general-purpose Bind-style models. Moreover, they often require full fine-tuning or supervised labels, making them incompatible with frozen-encoder architectures typical in foundation models.

To the best of our knowledge, we are the first to systematically investigate adversarial robustness in unified multi-modal foundation models. Our analysis (Table 1) reveals that both visual and non-visual modalities are highly vulnerable to adversarial perturbations. For instance, under an ℓ_∞ perturbation of $\epsilon = 2/255$, UniBind’s accuracy drops by 89.09% on ESC-50 (audio), 100% on ModelNet40 (point cloud), and 78.13% on LLVIP (thermal), compared to 95.11% on ImageNet-1K (image) and 51.01% on MSRVT (video). In addition, existing robust methods such as TeCo and FARE rely on retraining encoders or label supervision, which are infeasible for foundation models with frozen architectures.

To address this, we propose a lightweight adversarial calibration framework that enhances the robustness of Bind-style multi-modal models without modifying their encoders or semantic embedding space. We introduce modality-specific projection heads trained with adversarial samples, keeping the encoder and center embeddings entirely frozen. This plug-and-play design avoids disrupting cross-modal alignment and ensures compatibility with existing foundation models. We explore multiple objective functions within this frozen-encoder framework. (1) **Inspired by TeCo** [33], we implement a cross-entropy loss using fixed class-level semantic centers. (2) **Following the idea of FARE** [4], we apply an L2 loss that aligns adversarial embeddings to their clean counterparts without dynamic center updates. (3) We further explore a contrastive InfoNCE loss using clean–adversarial pairs. Building on these baselines, we propose a regularized variant that enforces modality-consistent alignment under adversarial perturbations. All objectives are trained without handcrafted prompts or paired cross-modal supervision; only the cross-entropy variant uses class labels.

To evaluate our method, we conduct extensive experiments across six modalities using three representative Bind-style models. For each model, we inherit frozen encoders and attach lightweight modality-specific MLP heads, trained using adversarial examples generated by AutoAttack under various ℓ_∞ perturbation budgets ($\epsilon = 2/255, 4/255, 8/255$). We assess both zero-shot classification and cross-modal retrieval to verify that robustness improvements do not come at the cost of alignment fidelity. We further compare standard MLP training with a parameter-efficient variant that incorporates LoRA, achieving favorable trade-offs between performance and efficiency. Our contributions are: (I) We present the first large-scale benchmark for adversarial robustness in unified multi-modal models, extending beyond vision-language tasks. (II) We propose a training framework that improves robustness while preserving pretrained encoders and semantic centers. (III) We introduce InfoNCE-based adversarial training for Bind models and compare it with cross-entropy and L2 objectives. (IV) We demonstrate that LoRA-enhanced projection heads enable efficient and effective robustness calibration without encoder modification.

2 Related Work

Adversarial Robustness in Vision-Language Models (CLIP): Adversarial robustness in vision-language models, particularly CLIP [29], has been widely studied. Despite strong zero-shot performance, CLIP remains highly vulnerable to adversarial perturbations [32]. To address this, various defenses have been proposed. TeCoA [32] introduces text-guided contrastive fine-tuning, while Wang et al. [35] enhance this with pre-trained feature regularization. Schlarmann et al. [34] propose RobustCLIP, an unsupervised method that aligns clean and adversarial embeddings without labels. Xing et al. [36] explore test-time defenses using CLIP’s own gradients. However, these approaches are limited to the image-text setting. *In contrast, our work extends adversarial robustness analysis and defenses to Bind-style models that support six or more sensory modalities.*

Bind-Style Multi-Modal Foundation Models aim to embed diverse sensory inputs into a shared semantic space [1, 3, 21, 37–41]. ImageBind [1] achieves cross-modal alignment using image-paired data. LanguageBind [3] aligns all modalities to a frozen text encoder with language annotations, while UniBind [4] introduces modality-agnostic alignment centers via large language models. While these models show strong zero-shot and retrieval performance, they have only been evaluated under clean conditions. Bagdasaryan et al. [37] identify ImageBind’s vulnerability to cross-modal attacks, but no prior work has explored adversarial robustness for LanguageBind or UniBind. *We provide the first systematic benchmark and adversarial training for Bind-style models, revealing critical vulnerabilities and introducing scalable defenses.*

Multi-Modal Adversarial Training and Evaluation: Recent studies have explored cross-modal attacks on multi-modal models. Bagdasaryan et al. [37] introduced adversarial illusions to misalign embeddings, while Dou et al. [42] proposed CrossFire, which converts a target input to the source modality before optimizing the perturbation. On the defense side, Waseda et al. [43] proposed Multi-modal Adversarial Training (MAT) for image-text retrieval using many-to-many data augmentations. However, these efforts are largely bimodal and often rely on handcrafted attacks or task-specific architectures. *Our work establishes a unified adversarial evaluation and training framework for Bind-style models across six modalities, addressing a key gap in multi-modal robustness.*

3 Methodology

3.1 Robustness of Bind Models

Bind-style multi-modal models encode inputs from different modalities into a shared embedding space. Given a modality $m \in \mathcal{M}$, let $\phi_m : X_m \rightarrow \mathbb{R}^D$ denote the encoder that maps inputs $x_m \in X_m$ to a shared D -dimensional space. In zero-shot classification settings, each class $k \in \{1, \dots, K\}$ is associated with a fixed semantic center $c_k \in \mathbb{R}^D$, either generated via language (e.g., in UniBind) or from LLM-based descriptions. Given a frozen encoder and semantic centers, each modality can be viewed as a fixed classifier:

$$f_k(\phi_m, x_m) = \cos \left(\frac{\phi_m(x_m)}{\|\phi_m(x_m)\|_2}, \frac{c_k}{\|c_k\|_2} \right) \quad (1)$$

The model predicts the class with the highest similarity:

$$\hat{y} = \arg \max_{k=1, \dots, K} f_k(\phi_m, x_m) \quad (2)$$

To evaluate adversarial robustness, we define an adversarial example x_m^{adv} as any input satisfying:

$$\arg \max_k f_k(\phi_m, x_m^{\text{adv}}) \neq y, \quad \|x_m^{\text{adv}} - x_m\|_p \leq \epsilon \quad (3)$$

where ϵ is the perturbation radius and $\|\cdot\|_p$ is typically chosen as ℓ_∞ . We employ AutoAttack [44] as a standardized attack to evaluate model robustness under this frozen classifier setting.

3.2 Projection Head Inheritance via Representation Distillation

Given a pretrained Bind-style model with a frozen encoder $\phi_m(\cdot)$ for modality m , we initialize a modality-specific projection head $h_m(\cdot)$ as a multi-layer perceptron (MLP). The goal of this stage is to distill the encoder’s clean output $z = \phi_m(x) \in \mathbb{R}^D$ into a lightweight MLP such that $\hat{z} = h_m(z) \approx z$, effectively preserving the semantic structure of the embedding space before adversarial training. This

define the L2 alignment loss as:

$$\mathcal{L}_{L2}(x^{\text{clean}}, x^{\text{adv}}) = \max_{\|x^{\text{adv}} - x^{\text{clean}}\|_{\infty} \leq \epsilon} \|h_m(\phi_m(x^{\text{adv}})) - h_m^{\text{target}}(\phi_m(x^{\text{clean}}))\|_2^2 \quad (5)$$

Given a dataset $\{x_i^{\text{clean}}\}_{i=1}^n$, we minimize the average L2 loss:

$$h_m^* = \arg \min_{h_m} \frac{1}{n} \sum_{i=1}^n \mathcal{L}_{L2}(x_i^{\text{clean}}, x_i^{\text{adv}}) \quad (6)$$

This formulation enforces adversarial embeddings to remain close to clean-space anchors established in Stage 1, while keeping the encoder and semantic centers frozen. Our two-stage pipeline naturally justifies omitting the clean loss term in Stage 2. Since the projection head h_m has already been trained with the self-distillation objective in Eq. 4, it effectively preserves clean representations over the encoder output space. Thus, the semantic geometry of clean features is maintained before adversarial training, making further clean supervision unnecessary.

Adversarial training often suffers from clean accuracy degradation due to catastrophic forgetting [46, 47], typically when the encoder is updated via adversarial gradients. In contrast, our framework keeps the encoder ϕ_m frozen, preserving clean representations and avoiding forgetting. Only the lightweight projection head is updated. Although Stage 2 omits a clean loss, the adversarial alignment objective implicitly regularizes the model. Despite a moderately large perturbation budget ($\epsilon = 8/255$), $\phi_m(x^{\text{adv}})$ remains near $\phi_m(x^{\text{clean}})$ in semantic space, and aligning $h_m(\phi_m(x^{\text{adv}}))$ to a fixed reference preserves clean-space alignment. This acts as input-adjacent regularization, promoting local smoothness and aiding clean accuracy retention. Empirically, adversarial-only training maintains strong clean performance, with improved generalization in modalities like audio and thermal. Our method simplifies training by removing the clean loss and dataset-specific tuning (as in FARE [34]), while preserving or improving clean accuracy. See Section 4.2 for details.

Supervised Adversarial Training with Cross-Entropy Loss

In addition to reconstruction-based objectives, we also explore a supervised adversarial training strategy using a fixed semantic classification layer. Let x^{clean} and x^{adv} denote a clean input and its adversarial version, and let $y \in \{1, \dots, K\}$ be its class label. We define a set of frozen semantic class centers $\{c_k\}_{k=1}^K \subset \mathbb{R}^D$, such as those derived from text embeddings in UniBind, and compute cosine similarity between the adversarial embedding and each center.

The classification logit for class k is defined as:

$$f_k(h_m, x^{\text{adv}}) = \cos \left(\frac{h_m(\phi_m(x^{\text{adv}}))}{\|h_m(\phi_m(x^{\text{adv}}))\|_2}, \frac{c_k}{\|c_k\|_2} \right), \quad (7)$$

and the resulting cross-entropy loss is:

$$\mathcal{L}_{\text{CE}}(y, x^{\text{adv}}) = -\log \frac{\exp(f_y(h_m, x^{\text{adv}}))}{\sum_{k=1}^K \exp(f_k(h_m, x^{\text{adv}}))}. \quad (8)$$

Given a labeled dataset $\{(x_i^{\text{clean}}, y_i)\}_{i=1}^n$, we optimize the projection head on adversarial samples via:

$$h_m^* = \arg \min_{h_m} \frac{1}{n} \sum_{i=1}^n \max_{\|x_i^{\text{adv}} - x_i^{\text{clean}}\|_{\infty} \leq \epsilon} \mathcal{L}_{\text{CE}}(y_i, x_i^{\text{adv}}). \quad (9)$$

The encoder remains frozen, with only the projection head trained. Unlike prior work like TeCoA [32], our approach avoids joint encoder training and token-level dropout, making it more lightweight and modular. While TeCoA [32] requires tuning clean-to-adversarial weighting and optimizing both vision and text branches, our method relies on frozen centers and trains only a small head. Despite its simplicity, our CE-based adversarial training achieves competitive or superior clean accuracy, particularly for high-resolution modalities like image and video. This indicates that adversarial calibration enhances robustness and sharpens clean decision boundaries, as discussed in Section 4.2.

Contrastive InfoNCE Loss for Adversarial Training To align clean and adversarial embeddings without class-level supervision, we use a contrastive objective based on the InfoNCE loss [45]. This encourages clean and adversarial embeddings from the same class to be similar, while pushing apart those from different classes. Let x^{clean} and x^{adv} denote a clean input and its adversarial version, both with class label $y \in \{1, \dots, K\}$. We concatenate these samples into a single batch of size $2n$ and compute their embeddings via a frozen encoder $\phi_m(\cdot)$ and a trainable projection head $h_m(\cdot)$. Let

$z_i = h_m(\phi_m(x_i)) \in \mathbb{R}^D$ denote the normalized embedding of sample i , and y_i its label. The cosine similarity between two embeddings is:

$$s_{i,j} = \frac{z_i^\top z_j}{\|z_i\|_2 \cdot \|z_j\|_2} \cdot \frac{1}{\tau}, \quad (10)$$

where τ is a temperature hyperparameter (typically 0.07). The InfoNCE loss is then:

$$\mathcal{L}_{\text{InfoNCE}} = -\frac{1}{2n} \sum_{i=1}^{2n} \log \frac{\sum_{j \neq i} \mathbb{I}[y_i = y_j] \cdot \exp(s_{i,j})}{\sum_{j \neq i} \exp(s_{i,j})}, \quad (11)$$

where $\mathbb{I}[\cdot]$ is an indicator function for positive pairs. The projection head is optimized via:

$$h_m^* = \arg \min_{h_m} \mathcal{L}_{\text{InfoNCE}}. \quad (12)$$

Unlike cross-entropy, which depends on global class alignment, InfoNCE relies solely on relative pairwise similarities, treating clean and adversarial instances equally. This local structure regularization often improves both robustness and clean accuracy, as discussed in Section 4.2 and Table 3. A theoretical robustness bound for the InfoNCE loss is provided in Appendix A.

3.4 LoRA-Based Parameter-Efficient Adaptation for Adversarial Fine-Tuning

To further reduce training overhead while improving robustness, we introduce a parameter-efficient variant of our adversarial framework using Low-Rank Adaptation (LoRA) [48]. LoRA enables efficient fine-tuning by injecting trainable low-rank matrices into existing linear layers, while keeping the original weights frozen. Let the projection head $h_m(\cdot)$ consist of a linear transformation with weight matrix $W_0 \in \mathbb{R}^{d_{\text{out}} \times d_{\text{in}}}$. Instead of updating W_0 directly, we reparameterize it using LoRA as:

$$W = W_0 + \alpha \cdot AB, \quad (13)$$

where $A \in \mathbb{R}^{d_{\text{out}} \times r}$ and $B \in \mathbb{R}^{r \times d_{\text{in}}}$ are trainable low-rank matrices with rank $r \ll \min(d_{\text{out}}, d_{\text{in}})$, and α is a tunable scalar scaling the update magnitude. During adversarial training, W_0 is frozen, and only A and B are updated using gradients.

Unlike recent methods such as AdvLoRA [49], which apply LoRA to multiple transformer layers and incorporate parameter clustering or reparameterization strategies, our approach inserts LoRA modules only into the projection head h_m , making it lightweight and easily transferable across modalities. This is particularly advantageous in Bind-style multi-modal models where the encoder is frozen and the projection head is modality-specific. We denote the adversarial objective with LoRA-enhanced projection head as:

$$\theta_{\text{LoRA}}^* = \arg \min_{\theta_{\text{LoRA}}} \mathcal{L}(x^{\text{adv}}, y), \quad (14)$$

where $\theta_{\text{LoRA}} = \{A, B\}$ are trainable parameters, and \mathcal{L} is the loss objective (*e.g.*, CE). A theoretical justification and additional analysis of the LoRA-injected projection head can be found in Appendix C.

4 Experiments

4.1 Quantitative Robustness Evaluation of Bind Models

Datasets and Modalities: We evaluate our method across six modalities using standard benchmarks. For images, we use ImageNet-1K [50] and Places365 [51]; for video, MSR-VTT [52] and UCF-101 [53]; for event data, N-ImageNet1K [54]; for point clouds, ModelNet40 [55]; for thermal images, LLVIP [56]; and for audio, ESC-50 [57]. To ensure at least two samples per class, we subsample 2000 evaluation examples for 1000-class datasets (*e.g.*, ImageNet-1K, N-ImageNet1K) and 1000 examples for the others. Training sets are five times the evaluation size, except for ESC-50, where the full dataset is used due to its smaller size.

Table 2: Overview of attack methods used during training and evaluation.

Attack Method	Type	Usage	ϵ
APGD-CE	Untargeted	Train + Eval	8 (train), 2/4/8 (eval)
APGD-DLR	Targeted	Eval only	2/4/8
FAB	Targeted	Eval only	2/4/8
Square	Black-box	Eval only	2/4/8

Attack Setup: We adopt AutoAttack [44] as our standard evaluation framework, using the four core attacks in its default suite: `apgd-ce`, `apgd-dlr`, `fab-t`, and `square`, with perturbation budgets

Table 1: Clean and adversarial accuracy (%) of UniBind, ImageBind, and LanguageBind across different modalities and datasets (subsamped, seed=42). \times indicates the modality is not supported.

Model	Setting	Image		Video		Event	Point	Thermal	Audio
		ImageNet1K	Places365	MSRVTT	UCF-101	N-ImageNet1K	ModelNet40	LLVIP	ESC-50
UniBind [4]	Clean	82.9	38.6	34.7	74.3	12.7	71.8	72.9	70.6
	AA ($\epsilon=2/255$)	4.0	0.6	17.0	20.3	6.2	0.0	8.9	7.7
	AA ($\epsilon=4/255$)	1.2	0.1	15.5	16.3	4.8	0.0	1.6	3.2
	AA ($\epsilon=8/255$)	0.3	0.0	13.7	12.5	2.7	0.0	0.2	1.5
ImageBind [1]	Clean	73.1	39.2	\times	\times	\times	\times	80.0	57.1
	AA ($\epsilon=2/255$)	3.0	1.2	\times	\times	\times	\times	17.5	6.9
	AA ($\epsilon=4/255$)	0.7	0.1	\times	\times	\times	\times	16.3	3.0
	AA ($\epsilon=8/255$)	0.1	0.0	\times	\times	\times	\times	15.4	1.2
LanguageBind [3]	Clean	75.4	42.2	43.6	71.5	\times	\times	80.3	94.7
	AA ($\epsilon=2/255$)	7.0	1.4	0.6	0.4	\times	\times	21.3	10.9
	AA ($\epsilon=4/255$)	1.6	0.4	0.0	0.0	\times	\times	18.3	4.1
	AA ($\epsilon=8/255$)	0.3	0.0	0.0	0.0	\times	\times	16.2	0.7

Table 3: Clean and adversarial Acc (%) of UniBind with different losses (L2, CE, InfoNCE) and LoRA (with/without, $r = 8$).

Loss Func	Modality	Image		Video		Event	Point	Thermal	Audio
	Dataset	ImgNet1K	Places365	MSRVTT	UCF-101	N-ImgNet1K	ModelNet40	LLVIP	ESC-50
L2	Clean	74.40 ↓8.5	34.90 ↓3.7	38.00 ↑3.3	75.10 ↑0.8	12.70 →0.0	47.80 ↓24.0	63.10 ↓9.8	19.50 ↓51.1
	AA (2/255)	8.65 ↑4.6	7.70 ↑7.1	22.60 ↑5.6	40.40 ↑20.1	7.95 ↑1.8	38.40 ↑38.4	70.70 ↑61.8	22.50 ↑14.8
	AA (4/255)	3.85 ↑2.6	5.60 ↑5.5	20.60 ↑5.1	38.10 ↑21.8	6.85 ↑2.0	44.90 ↑44.9	73.20 ↑71.6	28.20 ↑25.0
	AA (8/255)	2.70 ↑2.4	5.50 ↑5.5	19.20 ↑5.5	34.60 ↑22.1	4.70 ↑2.0	48.70 ↑48.7	75.20 ↑75.0	30.90 ↑29.4
L2+LoRA	Clean	81.75 ↓1.1	38.50 ↓0.1	36.50 ↑1.8	75.50 ↑1.2	12.65 ↓0.1	63.20 ↓8.6	62.50 ↓10.4	67.50 ↓3.1
	AA (2/255)	7.85 ↑3.8	3.00 ↑2.4	20.00 ↑5.6	26.70 ↑6.4	7.55 ↑1.8	19.20 ↑19.2	67.80 ↑58.9	15.50 ↑7.8
	AA (4/255)	3.55 ↑2.3	1.50 ↑1.4	18.70 ↑5.1	22.70 ↑6.4	6.50 ↑1.6	25.50 ↑25.5	70.80 ↑69.2	9.10 ↑5.9
	AA (8/255)	2.40 ↑2.1	1.20 ↑1.2	16.90 ↑5.5	18.00 ↑5.5	4.00 ↑1.3	31.90 ↑31.9	72.90 ↑72.7	4.90 ↑3.4
CE	Clean	63.80 ↓19.1	34.90 ↓3.7	62.90 ↑28.2	51.10 ↓23.2	14.05 ↑1.4	31.00 ↓40.8	74.50 ↑1.6	40.10 ↓30.5
	AA (2/255)	9.30 ↑5.2	12.10 ↑11.5	62.00 ↑45.0	48.50 ↑28.2	12.35 ↑6.2	53.40 ↑53.4	93.00 ↑84.1	35.40 ↑27.7
	AA (4/255)	5.85 ↑4.6	11.60 ↑11.5	61.30 ↑45.8	48.90 ↑32.6	12.00 ↑7.2	60.00 ↑60.0	97.60 ↑96.0	45.60 ↑42.4
	AA (8/255)	4.70 ↑4.4	11.50 ↑11.5	61.50 ↑47.8	48.70 ↑36.2	10.75 ↑8.1	61.50 ↑61.5	98.60 ↑98.4	48.30 ↑46.8
CE+LoRA	Clean	60.50 ↓22.4	35.90 ↓2.7	51.40 ↑16.7	47.40 ↓26.9	11.85 ↓0.8	19.40 ↓52.4	68.80 ↓4.1	70.50 ↓0.1
	AA (2/255)	7.45 ↑3.4	10.00 ↑9.4	49.70 ↑32.7	20.30 ↓0.0	9.15 ↑3.0	39.00 ↑39.0	92.20 ↑83.3	8.50 ↑0.8
	AA (4/255)	5.00 ↑3.8	9.10 ↑9.0	49.10 ↑33.6	18.30 ↑2.0	8.30 ↑3.5	44.80 ↑44.8	97.20 ↑95.6	4.10 ↑0.9
	AA (8/255)	4.10 ↑3.8	9.00 ↑9.0	49.00 ↑35.3	15.90 ↑3.4	6.85 ↑4.2	46.90 ↑46.9	98.80 ↑98.6	2.30 ↑0.8
InfoNCE	Clean	82.75 ↓0.1	36.70 ↓1.9	43.80 ↑9.1	73.40 ↓0.9	15.45 ↑2.8	49.60 ↓22.2	83.50 ↑10.6	63.50 ↓7.1
	AA (2/255)	14.50 ↑10.4	8.40 ↑7.8	36.10 ↑19.1	40.10 ↑19.8	12.65 ↑6.5	25.50 ↑25.5	42.30 ↑33.4	18.60 ↑10.9
	AA (4/255)	7.60 ↑6.3	7.20 ↑7.1	35.00 ↑19.5	36.80 ↑20.5	11.75 ↑6.9	32.60 ↑32.6	26.70 ↑25.1	18.60 ↑15.4
	AA (8/255)	5.25 ↑5.0	6.60 ↑6.6	34.00 ↑20.3	30.20 ↑17.7	10.10 ↑7.4	34.80 ↑34.8	17.60 ↑17.4	15.10 ↑13.6
InfoNCE+LoRA	Clean	82.75 ↓0.1	39.60 ↑1.0	45.50 ↑10.8	77.00 ↑2.7	14.70 ↑5.7	57.70 ↑10.0	77.10 ↑33.6	71.10 ↑1.5
	AA (2/255)	14.55 ↑10.5	9.10 ↑8.5	35.90 ↑18.9	39.40 ↑19.1	11.90 ↑5.7	10.00 ↑10.0	42.50 ↑33.6	9.20 ↑1.5
	AA (4/255)	7.50 ↑6.2	7.20 ↑7.1	34.30 ↑18.8	34.60 ↑18.3	10.85 ↑6.0	11.80 ↑11.8	36.20 ↑34.6	5.00 ↑1.8
	AA (8/255)	5.25 ↑5.0	6.60 ↑6.6	33.20 ↑19.5	28.10 ↑15.6	9.40 ↑6.7	15.20 ↑15.2	34.40 ↑34.2	2.90 ↑1.4

$\epsilon \in \{2, 4, 8\}/255$ under the ℓ_∞ norm. All six modalities—image, video, event, point cloud, thermal, and audio—are evaluated under these attacks, except for thermal. Due to its binary classification nature (LLVIP has only two classes), we exclude targeted attacks (apgd-dlr, fab-t) and apply only apgd-ce and square. During adversarial training, we use only apgd-ce with $\epsilon = 8/255$ for efficiency and generalizability, following findings that single-attack training at high ϵ can transfer well to other budgets [58–60]. See Table 2 for a summary of attack settings.

Models: We evaluate adversarial robustness across three multi-modal foundation models: *ImageBind* [1], *LanguageBind* [3], and *UniBind* [4].

Results and Discussion: Table 1 summarizes clean and adversarial accuracy under AutoAttack ($\epsilon \in \{2, 4, 8\}/255$). UniBind achieves the broadest coverage, strong clean accuracy (e.g., 82.90% on ImageNet1K), and relatively robust performance on video (e.g., 13.70% at $\epsilon = 8/255$), but fails on point cloud (0.00% even at $\epsilon = 2/255$). LanguageBind performs best on thermal (80.00% clean, 16.20% at $\epsilon = 8/255$) and audio (94.70% clean), but collapses completely on video under attack.

Table 4: Average acc (%) on LLVIP (thermal) and ESC-50 (audio) under different MLP sizes. Each value is the average across four loss-LoRA combinations (with and without LoRA, $r = 8$).

MLP Size	Loss Func	LLVIP (Thermal)	ESC-50 (Audio)
Small	L2	72.14	29.98
	CE	90.34	21.93
	InfoNCE	45.31	23.48
Medium	L2	69.53	24.76
	CE	90.09	31.85
	InfoNCE	45.04	25.50
Large	L2	70.20	34.34
	CE	89.51	22.16
	InfoNCE	48.35	24.10

Table 5: Average accuracy (%) on LLVIP (thermal) and ESC-50 (audio) under different LoRA ranks (r). Each value is averaged across three loss functions.

LoRA Rank	Loss Func	LLVIP (Thermal)	ESC-50 (Audio)
4	L2	66.90	23.60
	CE	89.85	21.60
	InfoNCE	50.20	21.75
8	L2	68.50	24.25
	CE	89.25	21.35
	InfoNCE	47.55	22.05
16	L2	66.63	24.45
	CE	89.90	21.28
	InfoNCE	48.48	21.93

ImageBind shows decent robustness on thermal (15.40% at $\epsilon = 8/255$) but lacks support for event and point data. All models perform poorly on image under adversarial perturbation, despite high clean accuracy. These results suggest that modality type significantly influences adversarial robustness, and that unified representation alone does not guarantee cross-modality resilience.

For a broader evaluation beyond accuracy, we also report **recall**, **precision**, and **F1-score** in Tables 6, 7, and 8, respectively. These metrics provide further insight into class-wise robustness and model reliability across clean and adversarial settings. Notably, performance drop patterns are consistent across all metrics, confirming that adversarial perturbations degrade not just accuracy but overall detection quality across modalities.

4.2 Adversarial Fine-Tuning

Two-Stage Adversarial Fine-Tuning Framework: We adopt a two-stage fine-tuning strategy to improve adversarial robustness while keeping the UniBind encoder frozen. In Stage 1, a lightweight MLP is trained to reconstruct the encoder’s clean embeddings via L_2 regression. This projection head then serves as initialization for Stage 2, which fine-tunes on offline-generated clean-adversarial pairs (AutoAttack, apgd-ce, $\epsilon = 8/255$). Inputs are reshaped to match modality-specific encoder formats. We compare three loss objectives: (1) L_2 loss to the frozen Stage-1 MLP (representation-level consistency), (2) cross-entropy loss with fixed class-level centers (semantic classification), and (3) InfoNCE loss with clean-adversarial positive pairs (contrastive alignment). For parameter-efficient training, we optionally insert LoRA adapters (rank $r = 8$) into the MLP. Models are trained for up to 30 epochs, with early stopping based on weighted accuracy ($0.25 \times \text{clean} + 0.75 \times \text{adversarial}$).

Table 3 compares the performance of different loss functions and LoRA configurations. InfoNCE achieves the highest clean accuracy (e.g., 82.75% on ImageNet1K, 83.50% on LLVIP) but struggles in robustness, especially on audio and point cloud. CE provides the best trade-off, maintaining high adversarial accuracy across modalities, especially thermal (e.g., 98.6% at $\epsilon = 8/255$) and video (e.g., 61.5% on MSRVT). **L2 loss performs worst**, collapsing quickly under attack. LoRA boosts clean accuracy in some cases (e.g., ESC-50: 70.5% with LoRA vs. 40.1%) but often reduces adversarial robustness, especially for InfoNCE. These results suggest that LoRA may overfit to clean representations without strong supervision (e.g., CE), and that loss type is critical for preserving adversarial alignment.

4.3 Ablation Study

Effect of MLP Size. Table 4 shows average accuracy on LLVIP and ESC-50 under three MLP sizes (small, medium, large), averaged across LoRA and non-LoRA variants. Cross-entropy remains stable across all sizes, suggesting that medium capacity is sufficient for alignment. Larger MLPs benefit L2 on audio (e.g., 34.34% for large vs. 24.76% for medium), but slightly hurts InfoNCE, likely due to overfitting. Overall, medium-sized MLPs achieve the best robustness-capacity trade-off. For the complete results across loss types and MLP widths, please refer to Table 10.

Effect of LoRA Rank. Table 5 compares LoRA ranks $r = 4, 8$, and 16. L2 and InfoNCE show sensitivity to rank, with peak robustness at $r = 8$ for L2 (68.50% on LLVIP) and $r = 4$ for InfoNCE (50.20%). CE again shows stability (89–90%) regardless of rank. On ESC-50, rank has minimal

impact across all loss functions. Thus, we recommend LoRA with $r = 8$ as a robust and efficient default configuration. For detailed accuracy breakdown across modalities and ranks, see Table 11.

Embedding space visualization with T-SNE.

Figure 3 compares encoder and MLP embeddings before and after adversarial training on LLVIP (Thermal). Encoder embeddings (left) show clear class separation but significant overlap under adversarial perturbations. In contrast, MLP embeddings (right) form compact, robust clusters, even at $\epsilon = 8/255$, indicating improved stability. To further quantify this improvement, we report the cosine similarity between clean and adversarial embeddings before and after fine-tuning in Table 9. Higher similarity—especially under cross-entropy (CE) training—demonstrates that the model effectively aligns adversarial features with their clean versions. In contrast, InfoNCE leads to larger embedding divergence on certain modalities (e.g., audio), despite strong clean accuracy. These results highlight the importance of loss function design not only for classification performance but also for maintaining embedding stability under adversarial threat.

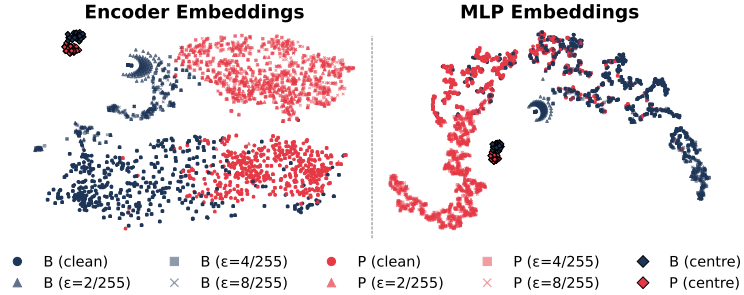


Figure 3: t-SNE visualization of embeddings before and after adversarial training. **Left:** Encoder embeddings show clear class separation and distinct perturbation levels (clean, $\epsilon=2/255$, $4/255$, $8/255$). **Right:** MLP embeddings after adversarial training form tighter, more robust clusters. Diamond markers denote class centers. Here, **P** and **B** represent the *person* and *background* classes, respectively.

5 Conclusion

In this work, we systematically studied the adversarial robustness of unified multi-modal foundation models, focusing on Bind-style architectures like UniBind, ImageBind, and LanguageBind. While these models excel in zero-shot performance under clean conditions, we find that they suffer significant degradation under mild adversarial perturbations, especially in non-visual modalities like audio, thermal, and point clouds. To address this, we propose a lightweight adversarial calibration framework that improves robustness without modifying pretrained encoders or semantic centers. Our study includes the first large-scale benchmark on adversarial robustness across six modalities and eight datasets, revealing severe vulnerabilities in non-visual inputs. We also introduce a two-stage fine-tuning framework that freezes the encoder, training only modality-specific projection heads to preserve the original embedding space. Additionally, we compare three loss objectives— L_2 alignment, cross-entropy with fixed centers, and InfoNCE—demonstrating that each offers different trade-offs between robustness and clean accuracy. Finally, we present a parameter-efficient variant using LoRA adapters for scalable robust fine-tuning, requiring less than 1% trainable parameters.

Limitations. While our framework is lightweight and compatible with existing foundation models, several limitations remain: (I) We focus on ℓ_∞ -bounded perturbations, but future work could explore other threat models like ℓ_2 , ℓ_1 , or spatial attacks. (II) Our approach assumes frozen encoders, which may be insufficient if encoder representations are significantly corrupted. (III) Generalization to unseen modalities or out-of-domain data remains unaddressed, highlighting the need for dynamic modality expansion in future work.

Broader Societal Impact. Our work aims to improve the adversarial robustness of multi-modal foundation models, which are increasingly deployed in real-world settings such as autonomous driving, robotics, and healthcare. Enhancing model robustness can mitigate potential risks from adversarial attacks in safety-critical environments. However, we acknowledge that robustness research can also inform adversarial offense strategies. This work is released with the intent to strengthen defenses and promote responsible AI development.

References

- [1] Rohit Girdhar, Alaaeldin El-Nouby, Zhuang Liu, Mannat Singh, Kalyan Vasudev Alwala, Armand Joulin, and Ishan Misra. Imagebind: One embedding space to bind them all. In *Proceedings of the IEEE/CVF Conference on Computer Vision and Pattern Recognition*, pages 14155–14165, 2023.
- [2] Bin Ren, Yahui Liu, Yue Song, Wei Bi, Rita Cucchiara, Nicu Sebe, and Wei Wang. Masked jigsaw puzzle: A versatile position embedding for vision transformers. In *Proceedings of the IEEE/CVF Conference on Computer Vision and Pattern Recognition*, pages 20382–20391, 2023.
- [3] Bin Zhu, Bin Lin, Munan Ning, Yang Yan, Jiayi Cui, HongFa Wang, Yatian Pang, Wenhao Jiang, Junwu Zhang, Zongwei Li, Wancai Zhang, Zhifeng Li, Wei Liu, and Li Yuan. Languagebind: Extending video-language pretraining to n-modality by language-based semantic alignment, 2024. URL <https://arxiv.org/abs/2310.01852>.
- [4] Yuanhuiyi Lyu, Xu Zheng, Jiazhou Zhou, and Lin Wang. Unibind: Llm-augmented unified and balanced representation space to bind them all. *arXiv preprint arXiv:2403.12532*, 2024.
- [5] Xu Zheng and Lin Wang. Eventdance: Unsupervised source-free cross-modal adaptation for event-based object recognition. In *Proceedings of the IEEE/CVF Conference on Computer Vision and Pattern Recognition*, pages 17448–17458, 2024.
- [6] Yuanhuiyi Lyu, Xu Zheng, Dahun Kim, and Lin Wang. Omnibind: Teach to build unequal-scale modality interaction for omni-bind of all. *arXiv preprint arXiv:2405.16108*, 2024.
- [7] Zehan Wang, Ziang Zhang, Xize Cheng, Rongjie Huang, Luping Liu, Zhenhui Ye, Haifeng Huang, Yang Zhao, Tao Jin, Peng Gao, et al. Freebind: Free lunch in unified multimodal space via knowledge fusion. *arXiv preprint arXiv:2405.04883*, 2024.
- [8] Xu Zheng, Yuanhuiyi Lyu, Jiazhou Zhou, and Lin Wang. Centering the value of every modality: Towards efficient and resilient modality-agnostic semantic segmentation. In *European Conference on Computer Vision*, pages 192–212. Springer, 2024.
- [9] Teng Xiao, Chao Cui, Huaisheng Zhu, and Vasant G Honavar. Molbind: Multimodal alignment of language, molecules, and proteins. *arXiv preprint arXiv:2403.08167*, 2024.
- [10] Adrian Mirza, Sebastian Starke, Erinc Merdivan, and Kevin Maik Jablonka. Bridging chemical modalities by aligning embeddings. In *AI for Accelerated Materials Design-Vienna 2024*, 2024.
- [11] Xu Zheng, Haiwei Xue, Jiale Chen, Yibo Yan, Lutao Jiang, Yuanhuiyi Lyu, Kailun Yang, Linfeng Zhang, and Xuming Hu. Learning robust anymodal segmentor with unimodal and cross-modal distillation. *arXiv preprint arXiv:2411.17141*, 2024.
- [12] Zhenqiang Li, Jie Li, Yangjie Cao, Jiayi Wang, and Runfeng Lv. Imagebind3d: Image as binding step for controllable 3d generation. In *Proceedings of the 32nd ACM International Conference on Multimedia*, pages 3362–3371, 2024.
- [13] Jiaming Han, Renrui Zhang, Wenqi Shao, Peng Gao, Peng Xu, Han Xiao, Kaipeng Zhang, Chris Liu, Song Wen, Ziyu Guo, et al. Imagebind-llm: Multi-modality instruction tuning. *arXiv preprint arXiv:2309.03905*, 2023.
- [14] Jiazhou Zhou, Xu Zheng, Yuanhuiyi Lyu, and Lin Wang. E-CLIP: towards label-efficient event-based open-world understanding by CLIP. *CoRR*, abs/2308.03135, 2023.
- [15] Jiahao Huo, Yibo Yan, Xu Zheng, Yuanhuiyi Lyu, Xin Zou, Zhihua Wei, and Xuming Hu. Mmunlearner: Reformulating multimodal machine unlearning in the era of multimodal large language models. *CoRR*, abs/2502.11051, 2025.
- [16] Bin Ren, Guofeng Mei, Danda Pani Paudel, Weijie Wang, Yawei Li, Mengyuan Liu, Rita Cucchiara, Luc Van Gool, and Nicu Sebe. Bringing masked autoencoders explicit contrastive properties for point cloud self-supervised learning. In *Proceedings of the Asian Conference on Computer Vision*, pages 2034–2052, 2024.

- [17] Yibo Yan, Jiamin Su, Jianxiang He, Fangteng Fu, Xu Zheng, Yuanhuiyi Lyu, Kun Wang, Shen Wang, Qingsong Wen, and Xuming Hu. A survey of mathematical reasoning in the era of multimodal large language model: Benchmark, method & challenges. *CoRR*, abs/2412.11936, 2024.
- [18] Bin Ren, Yawei Li, Jingyun Liang, Rakesh Ranjan, Mengyuan Liu, Rita Cucchiara, Luc V Gool, Ming-Hsuan Yang, and Nicu Sebe. Sharing key semantics in transformer makes efficient image restoration. *Advances in Neural Information Processing Systems*, 37:7427–7463, 2024.
- [19] Xu Zheng and Lin Wang. Eventdance++: Language-guided unsupervised source-free cross-modal adaptation for event-based object recognition. *CoRR*, abs/2409.12778, 2024.
- [20] Qi Ma, Yue Li, Bin Ren, Nicu Sebe, Ender Konukoglu, Theo Gevers, Luc Van Gool, and Danda Pani Paudel. Shapesplat: A large-scale dataset of gaussian splats and their self-supervised pretraining. In *International Conference on 3D Vision 2025*, 2024.
- [21] Xu Zheng, Yuanhuiyi Lyu, and Lin Wang. Learning modality-agnostic representation for semantic segmentation from any modalities. In *European Conference on Computer Vision*, pages 146–165. Springer, 2024.
- [22] Yuanhuiyi Lyu, Xu Zheng, and Lin Wang. Image anything: Towards reasoning-coherent and training-free multi-modal image generation. *arXiv preprint arXiv:2401.17664*, 2024.
- [23] Chenyang Zhu, Bin Xiao, Lin Shi, Shoukun Xu, and Xu Zheng. Customize segment anything model for multi-modal semantic segmentation with mixture of lora experts. *arXiv preprint arXiv:2412.04220*, 2024.
- [24] Koshiro Toishi, Keisuke Maeda, Ren Togo, Takahiro Ogawa, and Miki Haseyama. Improving zero-shot adversarial robustness via integrating image features of foundation models. In *2024 IEEE 13th Global Conference on Consumer Electronics (GCCE)*, pages 148–149. IEEE, 2024.
- [25] Aayush Dhakal, Subash Khanal, Srikumar Sastry, Adeel Ahmad, and Nathan Jacobs. Geobind: Binding text, image, and audio through satellite images. In *IGARSS 2024-2024 IEEE International Geoscience and Remote Sensing Symposium*, pages 2729–2733. IEEE, 2024.
- [26] Yuanhuiyi Lyu, Xu Zheng, Lutao Jiang, Yibo Yan, Xin Zou, Huiyu Zhou, Linfeng Zhang, and Xuming Hu. Realrag: Retrieval-augmented realistic image generation via self-reflective contrastive learning. *arXiv preprint arXiv:2502.00848*, 2025.
- [27] Xu Zheng, Ziqiao Weng, Yuanhuiyi Lyu, Lutao Jiang, Haiwei Xue, Bin Ren, Danda Paudel, Nicu Sebe, Luc Van Gool, and Xuming Hu. Retrieval augmented generation and understanding in vision: A survey and new outlook. *arXiv preprint arXiv:2503.18016*, 2025.
- [28] Chenfei Liao, Xu Zheng, Yuanhuiyi Lyu, Haiwei Xue, Yihong Cao, Jiawen Wang, Kailun Yang, and Xuming Hu. Memorysam: Memorize modalities and semantics with segment anything model 2 for multi-modal semantic segmentation. *arXiv preprint arXiv:2503.06700*, 2025.
- [29] Alec Radford, Jong Wook Kim, Chris Hallacy, Aditya Ramesh, Gabriel Goh, Sandhini Agarwal, Girish Sastry, Amanda Askell, Pamela Mishkin, Jack Clark, et al. Learning transferable visual models from natural language supervision. In *International conference on machine learning*, pages 8748–8763. PmLR, 2021.
- [30] Alex Fang, Gabriel Ilharco, Mitchell Wortsman, Yuhao Wan, Vaishaal Shankar, Achal Dave, and Ludwig Schmidt. Data determines distributional robustness in contrastive language image pre-training (clip). In *International Conference on Machine Learning (ICML)*, 2022.
- [31] Thao Nguyen, Gabriel Ilharco, Mitchell Wortsman, Sewoong Oh, and Ludwig Schmidt. Quality not quantity: On the interaction between dataset design and robustness of clip. In *Advances in Neural Information Processing Systems (NeurIPS)*, 2022.
- [32] Chengxu Mao, Yifan Wang, Yao Liu, Quanfu Fan, Xinyu Wang, Hong Xue, Xinyuan Wang, Xue Chen, Ming Liu, and Zhangyang Wang. Teco: Text-guided contrastive adversarial training for robust vision-language representation learning. In *Advances in Neural Information Processing Systems (NeurIPS)*, 2023.

- [33] Yuwei Lin, Pan Zhou, Xudong Chen, Mingming Xu, and Ji Wang. Teco: Token-aware robust contrastive learning for vision-language models. In *Proceedings of the IEEE/CVF International Conference on Computer Vision (ICCV)*, 2023.
- [34] Christian Schlarmann, Naman Deep Singh, Francesco Croce, and Matthias Hein. Robust clip: Unsupervised adversarial fine-tuning of vision embeddings for robust large vision-language models. In *International Conference on Machine Learning (ICML)*, 2024.
- [35] Sibow Wang, Jie Zhang, Zheng Yuan, and Shiguang Shan. Pre-trained model guided fine-tuning for zero-shot adversarial robustness. *arXiv preprint arXiv:2401.04350*, 2024.
- [36] Songlong Xing, Zhengyu Zhao, and Nicu Sebe. Clip is strong enough to fight back: Test-time counterattacks towards zero-shot adversarial robustness of clip. *arXiv preprint arXiv:2503.03613*, 2025.
- [37] Eugene Bagdasaryan et al. Adversarial illusions: Fooling multimodal foundation models. *arXiv preprint arXiv:2402.12336*, 2024.
- [38] Xu Zheng, Yexin Liu, Yunfan Lu, Tongyan Hua, Tianbo Pan, Weiming Zhang, Dacheng Tao, and Lin Wang. Deep learning for event-based vision: A comprehensive survey and benchmarks. *arXiv preprint arXiv:2302.08890*, 2023.
- [39] Jiazhou Zhou, Xu Zheng, Yuanhuiyi Lyu, and Lin Wang. Exact: Language-guided conceptual reasoning and uncertainty estimation for event-based action recognition and more. In *Proceedings of the IEEE/CVF Conference on Computer Vision and Pattern Recognition*, pages 18633–18643, 2024.
- [40] Jiazhou Zhou, Xu Zheng, Yuanhuiyi Lyu, and Lin Wang. Eventbind: Learning a unified representation to bind them all for event-based open-world understanding. In *European Conference on Computer Vision*, pages 477–494. Springer, 2024.
- [41] Xu Zheng, Yuanhuiyi Lyu, Lutao Jiang, Jiazhou Zhou, Lin Wang, and Xuming Hu. Magic++: Efficient and resilient modality-agnostic semantic segmentation via hierarchical modality selection. *arXiv preprint arXiv:2412.16876*, 2024.
- [42] Zhi Dou et al. Crossfire: A generalized multimodal adversarial attack. *arXiv preprint arXiv:2403.12345*, 2024.
- [43] Hiroshi Waseda et al. Multimodal adversarial training for vision-language models. *arXiv preprint arXiv:2405.18770*, 2024.
- [44] Francesco Croce and Matthias Hein. Reliable evaluation of adversarial robustness with an ensemble of diverse parameter-free attacks. In *International conference on machine learning*, pages 2206–2216. PMLR, 2020.
- [45] Aaron van den Oord, Yazhe Li, and Oriol Vinyals. Representation learning with contrastive predictive coding. *arXiv preprint arXiv:1807.03748*, 2018.
- [46] Ian J Goodfellow, Jonathon Shlens, and Christian Szegedy. Explaining and harnessing adversarial examples. In *International Conference on Learning Representations (ICLR)*, 2015.
- [47] Dimitris Tsipras, Shibani Santurkar, Logan Engstrom, Brandon Turner, and Aleksander Madry. Robustness may be at odds with accuracy. In *International Conference on Learning Representations (ICLR)*, 2019.
- [48] Edward J Hu, Yelong Shen, Phil Wallis, Zeyuan Allen-Zhu, Yuanzhi Li, Shean Wang, and Wei Ping. Lora: Low-rank adaptation of large language models. In *International Conference on Learning Representations (ICLR)*, 2022. URL <https://arxiv.org/abs/2106.09685>.
- [49] Yuheng Ji, Yue Liu, Zhicheng Zhang, et al. Advlora: Adversarial low-rank adaptation of vision-language models. *arXiv preprint arXiv:2404.13425*, 2024.
- [50] Jia Deng, Wei Dong, Richard Socher, Li-Jia Li, Kai Li, and Li Fei-Fei. Imagenet: A large-scale hierarchical image database. *CVPR*, 2009.

- [51] Bolei Zhou, Agata Lapedriza, Aditya Khosla, Aude Oliva, and Antonio Torralba. Places: A 10 million image database for scene recognition. *IEEE Transactions on Pattern Analysis and Machine Intelligence*, 2017.
- [52] Jun Xu, Tao Mei, Ting Yao, and Yong Rui. Msr-vtt: A large video description dataset for bridging video and language. In *CVPR*, 2016.
- [53] Khurram Soomro, Amir Roshan Zamir, and Mubarak Shah. Ucf101: A dataset of 101 human actions classes from videos in the wild. In *CRCV-TR-12-01*, 2012.
- [54] Daniel Gehrig, Henri Rebecq, Guillermo Gallego, and Davide Scaramuzza. Dsec: A stereo event camera dataset for driving scenarios. In *RA-L / ICRA*, 2021.
- [55] Zhirong Wu, Shuran Song, Aditya Khosla, Fisher Yu, Linguang Zhang, Xiaoou Tang, and Jianxiong Xiao. 3d shapenets: A deep representation for volumetric shapes. In *CVPR*, 2015.
- [56] Yu Wang, Jiawei Zhang, Xuequan Lu, Qingjie Zhao, and Liang Zhang. Llvip: A visible-infrared paired dataset for low-light vision. In *ACM MM*, 2021.
- [57] Karol J Piczak. Esc: Dataset for environmental sound classification. In *ACM Multimedia*, 2015.
- [58] Sylvestre-Alvise Rebuffi, Felix Dangel, and Andrew Zisserman. Fixing data augmentation to improve adversarial robustness. In *NeurIPS*, 2021.
- [59] Sven Gowal, Chongli Qin, Jonathan Uesato, Timothy Mann, and Pushmeet Kohli. Uncovering the limits of adversarial training against norm-bounded adversarial examples. In *ICML*, 2020.
- [60] Hongyang Zhang, Yaodong Yu, Jiantao Jiao, Eric Xing, Laurent El Ghaoui, and Michael Jordan. Theoretically principled trade-off between robustness and accuracy. In *ICML*, 2019.

Contents of Appendix

- A. Proof of InfoNCE-based Robustness Bound
- B. Two-Stage Training Justification
- C. LoRA-Injected Projection Head
- D. Experiments
- E. License

A Proof of InfoNCE-based Robustness Bound

Theorem (InfoNCE Robustness Bound). Let ϕ_{Org}, ϕ_{FT} denote original and fine-tuned image embeddings, and ψ denote text embeddings. Let $\mathcal{L}_{\text{InfoNCE}}$ denote the InfoNCE loss:

$$\mathcal{L}_{\text{InfoNCE}}(\phi, \psi) = -\frac{1}{N} \sum_{i=1}^N \log \frac{e^{\cos(\phi(x_i), \psi(t_i))/\tau}}{\sum_{j=1}^N e^{\cos(\phi(x_i), \psi(t_j))/\tau}}. \quad (15)$$

Then the following bound holds:

$$|\mathcal{L}_{\text{InfoNCE}}(\phi_{FT}, \psi) - \mathcal{L}_{\text{InfoNCE}}(\phi_{Org}, \psi)| \leq C \cdot \frac{2}{\tau \min_i \|\phi_{Org}(x_i)\|_2} \sum_{i=1}^N \|\phi_{FT}(x_i) - \phi_{Org}(x_i)\|_2, \quad (16)$$

where C is a constant dependent on batch size N and Lipschitz constant of the exponential function.

Proof. For simplicity, define:

$$a_i^{FT} = \frac{\cos(\phi_{FT}(x_i), \psi(t_i))}{\tau}, \quad a_i^{Org} = \frac{\cos(\phi_{Org}(x_i), \psi(t_i))}{\tau},$$

$$b_{ij}^{FT} = \frac{\cos(\phi_{FT}(x_i), \psi(t_j))}{\tau}, \quad b_{ij}^{Org} = \frac{\cos(\phi_{Org}(x_i), \psi(t_j))}{\tau}.$$

Consider the i -th term of the InfoNCE difference:

$$\Delta_i = \left| \log \frac{e^{a_i^{FT}}}{\sum_{j=1}^N e^{b_{ij}^{FT}}} - \log \frac{e^{a_i^{Org}}}{\sum_{j=1}^N e^{b_{ij}^{Org}}} \right| \quad (17)$$

$$\leq |a_i^{FT} - a_i^{Org}| + \left| \log \frac{\sum_{j=1}^N e^{b_{ij}^{FT}}}{\sum_{j=1}^N e^{b_{ij}^{Org}}} \right|. \quad (18)$$

Using Lipschitz continuity of the exponential function with constant L_e :

$$|e^{b_{ij}^{FT}} - e^{b_{ij}^{Org}}| \leq L_e |b_{ij}^{FT} - b_{ij}^{Org}|,$$

we have:

$$\left| \sum_{j=1}^N (e^{b_{ij}^{FT}} - e^{b_{ij}^{Org}}) \right| \leq L_e \sum_{j=1}^N |b_{ij}^{FT} - b_{ij}^{Org}|.$$

Thus:

$$\left| \log \frac{\sum_{j=1}^N e^{b_{ij}^{FT}}}{\sum_{j=1}^N e^{b_{ij}^{Org}}} \right| \leq \frac{L_e \sum_{j=1}^N |b_{ij}^{FT} - b_{ij}^{Org}|}{\min(\sum_j e^{b_{ij}^{FT}}, \sum_j e^{b_{ij}^{Org}})}. \quad (19)$$

Further, using the cosine similarity bound from original theorem:

$$|\cos(\phi_{FT}(x_i), \psi(t_j)) - \cos(\phi_{Org}(x_i), \psi(t_j))| \leq \frac{2}{\|\phi_{Org}(x_i)\|_2} \|\phi_{FT}(x_i) - \phi_{Org}(x_i)\|_2,$$

we have:

$$|b_{ij}^{FT} - b_{ij}^{Org}| \leq \frac{2}{\tau \|\phi_{Org}(x_i)\|_2} \|\phi_{FT}(x_i) - \phi_{Org}(x_i)\|_2. \quad (20)$$

Summing over i and collecting terms, we obtain:

$$|\mathcal{L}_{\text{InfoNCE}}(\phi_{FT}, \psi) - \mathcal{L}_{\text{InfoNCE}}(\phi_{Org}, \psi)| \leq \frac{2C}{\tau \min_i \|\phi_{Org}(x_i)\|_2} \sum_{i=1}^N \|\phi_{FT}(x_i) - \phi_{Org}(x_i)\|_2, \quad (21)$$

where C combines constants related to batch size and exponential Lipschitz continuity.

This completes the proof. \square

B Two-Stage Training Justification

Our adversarial calibration framework employs a two-stage training pipeline designed to preserve the semantic structure of the shared embedding space while improving adversarial robustness with minimal overhead.

Let $\phi(\cdot)$ be a frozen encoder and $z = \phi(x)$ denote the clean input embedding. In **Stage 1**, we train a modality-specific MLP $h_1(\cdot)$ using clean samples by minimizing a self-reconstruction loss:

$$\mathcal{L}_{\text{distill}} = \|h_1(\phi(x)) - \phi(x)\|_2^2. \quad (22)$$

This step distills the semantic structure from the frozen encoder into a lightweight projection head, producing a clean-aligned head h_1 that approximates the identity mapping over $\phi(x)$.

In **Stage 2**, a separate MLP h_2 is initialized (optionally from h_1) and trained using adversarial samples x^{adv} by minimizing:

$$\mathcal{L}_{\text{adv}} = \|h_2(\phi(x^{\text{adv}})) - h_1(\phi(x))\|_2^2. \quad (23)$$

This encourages the adversarial representation to align with the clean semantic embedding defined by h_1 . Importantly, we omit the clean loss in Stage 2. We justify this by showing that the adversarial output of h_2 remains close to the clean embedding $z = \phi(x)$ via the triangle inequality:

$$\|h_2(\phi(x^{\text{adv}})) - \phi(x)\|_2 \leq \|h_2(\phi(x^{\text{adv}})) - h_1(\phi(x))\|_2 + \|h_1(\phi(x)) - \phi(x)\|_2. \quad (24)$$

The second term is minimized during Stage 1 and thus small by construction. Hence, minimizing \mathcal{L}_{adv} indirectly constrains adversarial embeddings to remain close to their clean counterparts.

Moreover, since both ϕ and h_1 are fixed, this training process is stable and avoids the catastrophic forgetting commonly observed in encoder-updating adversarial training. The clean representation structure is preserved throughout, and only robustness calibration is performed.

This two-stage strategy decouples semantic preservation from robustness learning, allowing for modular training, stable optimization, and efficient parameter reuse across modalities. It also enables the use of adversarial-only objectives in Stage 2, reducing the need for balancing clean vs. adversarial terms in the loss function.

C LoRA-Injected Projection Head

To further reduce the training overhead of adversarial calibration, we adopt Low-Rank Adaptation (LoRA) for parameter-efficient fine-tuning of projection heads. Specifically, we decompose a linear layer weight $W \in \mathbb{R}^{d_{\text{out}} \times d_{\text{in}}}$ into a frozen base matrix W_0 and a trainable low-rank component:

$$W = W_0 + \alpha \cdot AB, \quad A \in \mathbb{R}^{d_{\text{out}} \times r}, \quad B \in \mathbb{R}^{r \times d_{\text{in}}}, \quad r \ll \min(d_{\text{out}}, d_{\text{in}}), \quad (25)$$

where α is a scaling factor and A, B are trainable parameters. Only A and B are updated during training, while W_0 remains frozen.

This setup introduces a constrained subspace hypothesis class:

$$\mathcal{H}_{\text{LoRA}} = \{W_0 + \alpha AB : A \in \mathbb{R}^{d_{\text{out}} \times r}, B \in \mathbb{R}^{r \times d_{\text{in}}}\}. \quad (26)$$

Although this space is significantly lower-dimensional than the full space of $W \in \mathbb{R}^{d_{\text{out}} \times d_{\text{in}}}$, prior theoretical work (*e.g.*, Hu et al. 2022) shows that low-rank updates suffice to approximate the effect of full fine-tuning under smooth loss landscapes and overparameterized regimes.

In our context, where the encoder $\phi(\cdot)$ is frozen and the projection head is the only trainable module, LoRA provides three important benefits:

1. **Preservation of Semantic Geometry:** Since W_0 preserves the initialization from Stage 1 (clean-aligned), the low-rank updates do not drastically distort semantic directions in the embedding space.
2. **Robustness Alignment:** The adversarial training objective (*e.g.*, L2 or InfoNCE) applied on the LoRA-augmented projection head still optimizes:

$$\min_{A, B} \mathcal{L}_{\text{adv}}(W_0 + \alpha AB) \quad (27)$$

where the optimization is over a smoother, smaller parameter manifold, often yielding better generalization.

3. **Controlled Update Norm:** Due to the low-rank structure, the induced change in the model output is bounded. Specifically, the Frobenius norm of the update is:

$$\|\alpha AB\|_F \leq \alpha \cdot \|A\|_F \cdot \|B\|_F \quad (28)$$

allowing us to regularize the perturbation explicitly.

Together, these properties ensure that LoRA can calibrate adversarial robustness effectively while minimizing interference with the clean-space alignment established in Stage 1. Empirical results (*e.g.*, Table 10) confirm that LoRA-enhanced heads match or exceed performance of full-rank MLPs with significantly fewer parameters and less training time.

D Experiments

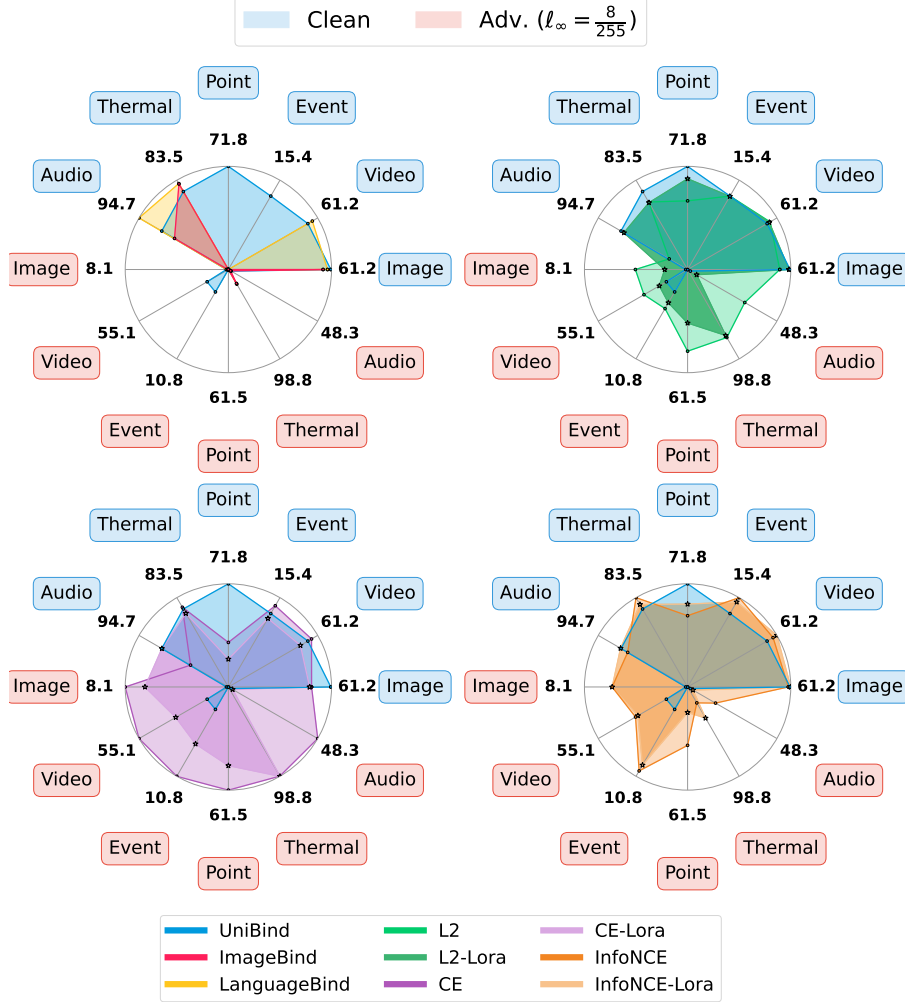


Figure 4: Radar charts showing clean and adversarial accuracy ($\ell_\infty = 8/255$) across six modalities: Image, Video, Event, Point, Thermal, and Audio. From left to right: (1) Three foundation models—UniBind, ImageBind, and LanguageBind; (2) UniBind, CE, and CE+LoRA; (3) UniBind, InfoNCE, and InfoNCE+LoRA; (4) UniBind, L2, and L2+LoRA. Blue areas represent clean accuracy, while red areas indicate adversarial performance under $\ell_\infty = 8/255$ perturbation.

Compute Resources. All experiments were conducted on a single NVIDIA RTX 4090 GPU. Training each modality-specific MLP head required less than 3 GPU-hours on average, except for the video modality, which required approximately 16 GPU-hours due to higher input dimensionality and slower augmentation. Total training time across all configurations (including loss variations and LoRA ranks) remained under 100 GPU-hours. No distributed or multi-node setup was used.

Table 6: Clean and adversarial **recall** (%) of UniBind, ImageBind, and LanguageBind across different modalities and datasets (subsamped, seed=42). **X** indicates the modality is not supported.

Model	Setting	Image		Video		Event	Point	Thermal	Audio
		ImageNet1K	Places365	MSRVTT	UCF-101	N-ImageNet1K	ModelNet40	LLVIP	ESC-50
UniBind [4]	Clean	83.09	40.39	30.30	73.83	12.37	61.23	72.54	70.84
	AA ($\epsilon=2/255$)	3.67	0.46	14.88	20.41	6.15	0.00	8.69	7.78
	AA ($\epsilon=4/255$)	1.20	0.07	13.71	16.60	5.05	0.00	1.57	3.30
	AA ($\epsilon=8/255$)	0.30	0.00	11.90	13.01	2.83	0.00	0.19	1.52
ImageBind [1]	Clean	73.65	41.19	X	X	X	X	79.75	57.09
	AA ($\epsilon=2/255$)	2.95	0.86	X	X	X	X	18.16	6.98
	AA ($\epsilon=4/255$)	0.74	0.07	X	X	X	X	16.85	3.30
	AA ($\epsilon=8/255$)	0.13	0.00	X	X	X	X	15.84	1.24
LanguageBind [3]	Clean	75.97	43.52	40.50	69.81	X	X	80.02	94.31
	AA ($\epsilon=2/255$)	6.85	1.16	0.65	0.43	X	X	21.91	11.12
	AA ($\epsilon=4/255$)	1.51	0.35	0.00	0.00	X	X	18.83	4.18
	AA ($\epsilon=8/255$)	0.28	0.00	0.00	0.00	X	X	16.67	0.72

Table 7: Clean and adversarial **precision** (%) of UniBind, ImageBind, and LanguageBind across different modalities and datasets (subsamped, seed=42). **X** indicates the modality is not supported.

Model	Setting	Image		Video		Event	Point	Thermal	Audio
		ImageNet1K	Places365	MSRVTT	UCF-101	N-ImageNet1K	ModelNet40	LLVIP	ESC-50
UniBind [4]	Clean	81.37	39.73	37.47	76.52	13.28	58.32	74.29	69.20
	AA ($\epsilon=2/255$)	4.27	0.74	19.79	37.35	6.17	0.00	8.01	7.80
	AA ($\epsilon=4/255$)	1.20	0.15	18.36	33.16	4.76	0.00	1.60	3.09
	AA ($\epsilon=8/255$)	0.21	0.00	16.75	27.69	2.35	0.00	0.20	1.69
ImageBind [1]	Clean	71.00	42.14	X	X	X	X	82.32	57.87
	AA ($\epsilon=2/255$)	3.63	1.48	X	X	X	X	13.03	9.52
	AA ($\epsilon=4/255$)	1.09	0.29	X	X	X	X	12.32	6.61
	AA ($\epsilon=8/255$)	0.15	0.00	X	X	X	X	11.53	3.38
LanguageBind [3]	Clean	73.62	42.44	44.43	70.05	X	X	81.49	95.57
	AA ($\epsilon=2/255$)	6.49	1.43	0.65	0.28	X	X	14.65	10.72
	AA ($\epsilon=4/255$)	1.41	0.52	0.00	0.00	X	X	13.13	3.59
	AA ($\epsilon=8/255$)	0.24	0.00	0.00	0.00	X	X	11.98	1.11

Table 8: Clean and adversarial **F1-score** (%) of UniBind, ImageBind, and LanguageBind across different modalities and datasets (subsamped, seed=42). **X** indicates the modality is not supported.

Model	Setting	Image		Video		Event	Point	Thermal	Audio
		ImageNet1K	Places365	MSRVTT	UCF-101	N-ImageNet1K	ModelNet40	LLVIP	ESC-50
UniBind [4]	Clean	80.12	36.75	30.64	72.94	10.84	58.76	72.28	67.56
	AA ($\epsilon=2/255$)	3.55	0.54	14.38	22.54	5.17	0.00	8.33	5.96
	AA ($\epsilon=4/255$)	1.06	0.10	13.08	18.87	4.17	0.00	1.59	2.65
	AA ($\epsilon=8/255$)	0.18	0.00	11.64	14.56	2.08	0.00	0.20	1.41
ImageBind [1]	Clean	69.51	37.55	X	X	X	X	79.50	53.00
	AA ($\epsilon=2/255$)	2.79	0.97	X	X	X	X	15.17	6.57
	AA ($\epsilon=4/255$)	0.77	0.09	X	X	X	X	14.23	2.91
	AA ($\epsilon=8/255$)	0.14	0.00	X	X	X	X	13.34	1.30
LanguageBind [3]	Clean	72.08	39.16	39.05	67.10	X	X	80.00	94.33
	AA ($\epsilon=2/255$)	5.84	1.16	0.44	0.29	X	X	17.56	7.65
	AA ($\epsilon=4/255$)	1.31	0.36	0.00	0.00	X	X	15.47	2.36
	AA ($\epsilon=8/255$)	0.22	0.00	0.00	0.00	X	X	15.47	0.36

Table 9: Average cosine similarity (%) to the same-class center embedding across different loss functions and adversarial perturbation levels, evaluated on various modalities and datasets (subsamped, seed=42).

Method	Setting	Image		Video		Event	Point	Thermal	Audio
		ImageNet1K	Places-Stanford	MSRVTT	UCF-101	N-ImageNet1K	ModelNet40	LLVIP	ESC-50
UniBind	Clean	34.13	26.91	28.31	35.42	23.21	22.51	10.26	27.95
	AA ($\epsilon=2/255$)	20.46	22.18	26.52	28.99	22.96	12.86	10.19	12.21
	AA ($\epsilon=4/255$)	13.98	19.42	26.33	28.38	22.85	11.98	11.90	8.51
	AA ($\epsilon=8/255$)	5.26	16.22	26.11	27.61	22.59	11.83	13.78	4.98
L2	Clean	20.62	23.47	28.75	57.51	23.20	19.28	23.03	19.14
	AA ($\epsilon=2/255$)	16.49	19.24	28.37	31.83	23.02	18.62	10.07	19.88
	AA ($\epsilon=4/255$)	15.58	18.12	28.29	31.40	22.93	18.01	10.25	21.94
	AA ($\epsilon=8/255$)	14.24	17.00	28.14	30.75	22.71	17.52	10.49	19.31
CE	Clean	26.82	41.46	52.12	53.67	33.76	32.51	50.89	44.98
	AA ($\epsilon=2/255$)	26.28	33.69	51.54	50.47	33.46	38.75	43.21	47.28
	AA ($\epsilon=4/255$)	26.83	32.05	52.62	50.60	33.33	39.58	37.39	49.84
	AA ($\epsilon=8/255$)	30.70	30.30	51.56	50.93	32.95	40.66	37.58	52.59
InfoNCE	Clean	26.73	16.05	18.60	24.53	15.39	12.38	6.58	16.17
	AA ($\epsilon=2/255$)	12.77	12.76	17.70	20.22	15.09	10.06	5.92	7.96
	AA ($\epsilon=4/255$)	6.80	10.95	17.55	19.41	14.95	10.10	7.05	6.57
	AA ($\epsilon=8/255$)	-0.32	8.91	17.35	18.23	14.58	10.11	7.49	4.43

Table 10: Accuracy (%) of adversarial settings across loss functions, LoRA, and MLP sizes on LLVIP (Thermal) and ESC-50 (Audio) datasets (1000 samples, seed=42).

Loss Func	LoRA	Dataset MLP Size	LLVIP (Thermal)			ESC-50 (Audio)		
			Small	Medium	Large	Small	Medium	Large
L2	FALSE	Clean	76.20	63.10	67.50	50.80	19.50	38.80
		AA ($\epsilon=2/255$)	72.50	70.70	71.80	29.10	22.50	35.20
		AA ($\epsilon=4/255$)	74.10	73.20	73.90	34.30	28.20	44.70
		AA ($\epsilon=8/255$)	76.20	75.20	75.50	33.70	30.90	48.50
	R=8	Clean	63.70	62.50	74.70	66.00	67.50	63.40
		AA ($\epsilon=2/255$)	68.70	67.80	68.30	13.50	15.50	17.70
		AA ($\epsilon=4/255$)	71.60	70.80	65.10	7.30	5.10	15.70
		AA ($\epsilon=8/255$)	74.10	72.90	64.80	4.60	4.90	10.70
CE	FALSE	Clean	73.40	74.50	71.20	23.40	40.10	17.30
		AA ($\epsilon=2/255$)	92.70	93.00	92.40	19.80	35.40	23.30
		AA ($\epsilon=4/255$)	97.30	97.60	97.10	23.40	45.60	28.10
		AA ($\epsilon=8/255$)	98.50	98.60	98.60	26.50	48.30	28.10
	R=8	Clean	75.20	68.80	72.40	71.00	70.50	60.60
		AA ($\epsilon=2/255$)	91.40	92.20	91.10	3.50	3.50	5.50
		AA ($\epsilon=4/255$)	96.20	97.20	95.50	4.30	4.10	4.30
		AA ($\epsilon=8/255$)	98.00	98.80	97.80	2.40	2.30	3.20
InfoNCE	FALSE	Clean	87.30	83.50	81.60	68.70	63.50	62.70
		AA ($\epsilon=2/255$)	31.80	42.30	43.30	15.70	13.60	17.60
		AA ($\epsilon=4/255$)	21.70	26.70	35.30	10.20	13.60	14.60
		AA ($\epsilon=8/255$)	19.50	17.60	33.20	7.00	15.10	11.90
	R=8	Clean	26.70	77.10	76.60	68.10	71.10	70.60
		AA ($\epsilon=2/255$)	44.50	42.50	43.40	9.30	9.20	2.30
		AA ($\epsilon=4/255$)	36.60	36.20	36.20	5.00	5.00	4.40
		AA ($\epsilon=8/255$)	34.40	34.40	36.70	2.70	2.90	2.20

Table 11: Accuracy (%) of adversarial settings across loss functions and LoRA ranks (R=4, 8, 16) on LLVIP (Thermal) and ESC-50 (Audio) datasets (1000 samples, seed=42).

Loss Func	Dataset LoRA	LLVIP (Thermal)			ESC-50 (Audio)		
		R=4	R=8	R=16	R=4	R=8	R=16
L2	Clean	62.20	62.50	74.00	66.90	67.50	66.40
	AA ($\epsilon=2/255$)	66.70	67.80	67.90	15.30	15.50	16.00
	AA ($\epsilon=4/255$)	68.80	70.80	65.60	7.90	9.10	10.40
	AA ($\epsilon=8/255$)	69.90	72.90	59.00	4.30	4.90	5.00
CE	Clean	75.10	68.80	74.30	70.40	70.50	70.20
	AA ($\epsilon=2/255$)	90.70	92.20	91.10	9.10	8.50	8.50
	AA ($\epsilon=4/255$)	95.90	97.20	96.30	4.40	4.10	4.20
	AA ($\epsilon=8/255$)	97.70	98.80	97.90	2.50	2.30	2.20
InfoNCE	Clean	84.00	77.10	81.10	70.60	71.10	70.90
	AA ($\epsilon=2/255$)	44.20	42.50	42.70	8.90	9.20	9.10
	AA ($\epsilon=4/255$)	37.10	36.20	36.10	4.30	5.00	5.00
	AA ($\epsilon=8/255$)	35.50	34.40	34.00	2.70	2.90	2.70

This appendix provides additional quantitative results across multiple datasets, modalities, and robustness settings.

Table 6 – Recall. This table reports clean and adversarial recall scores for UniBind, ImageBind, and LanguageBind. UniBind maintains stable recall across most modalities, especially in thermal and audio. LanguageBind achieves the highest recall in clean conditions but degrades faster under adversarial perturbations. ImageBind, while limited in modality support, performs well on thermal.

Table 7 – Precision. Precision trends are similar to recall. LanguageBind demonstrates strong performance on ESC-50 (audio), remaining stable under high perturbations. UniBind provides reasonable stability across modalities. ImageBind achieves the highest clean precision in thermal but is more sensitive to attacks.

Table 8 – F1-score. F1-score, as a harmonic mean of precision and recall, highlights overall performance. UniBind shows stronger robustness in thermal. LanguageBind dominates audio performance under all ϵ settings. ImageBind suffers the most in F1-score when faced with perturbations.

Table 9 – Cosine Similarity to Same-Class Centers. This table reports the average cosine similarity between each sample’s embedding and its corresponding class center across different loss functions and adversarial perturbations. UniBind achieves the highest cosine similarity under clean conditions in most modalities, indicating strong intra-class alignment. However, it degrades rapidly under attack, especially in vision-related modalities. In contrast, CE-trained models demonstrate more stable alignment across all perturbation levels, particularly in video and thermal, where similarity remains high even under $\epsilon = 8/255$. L2 shows moderate robustness, while InfoNCE suffers the sharpest decline—dropping to negative similarity on ImageNet1K. Overall, CE offers the best trade-off between clean performance and robustness, outperforming UniBind and InfoNCE in adversarial settings.

Table 10 – Accuracy across Loss Functions, LoRA, and MLP Sizes. This table evaluates the effects of different training losses (L2, CE, InfoNCE), LoRA configurations, and MLP sizes. CE loss combined with LoRA (R=8) achieves the best adversarial accuracy (*e.g.*, over 98% in LLVIP). InfoNCE improves robustness in LLVIP but fluctuates in ESC-50. LoRA generally improves performance across losses, especially with CE.

Table 11 – Accuracy vs. LoRA Rank. This table studies the effect of LoRA rank (R=4,8,16). CE loss performs consistently across all ranks, showing little sensitivity to rank. InfoNCE is more sensitive to rank changes, with performance improving at higher ranks. L2 is relatively less influenced by rank.

E License

Table 12: Licenses for all datasets and models used in this work.

Asset	License	Used For
ImageNet-1K [50]	Custom Academic License	Image Modality
Places365 [51]	MIT License	Image Modality
ESC-50 [57]	CC BY 4.0	Audio Modality
LLVIP [56]	For Research Use Only	Thermal Modality
MSRVTT [52]	Academic Use License	Video Modality
UCF-101 [53]	Academic Use License	Video Modality
N-ImageNet1K [54]	For Research Use Only	Event Modality
ModelNet40 [55]	Unknown / Academic Use	Point Cloud Modality
UniBind [4]	MIT License (GitHub)	Base Model
ImageBind [1]	CC-BY-NC 4.0	Base Model
LanguageBind [3]	MIT License (GitHub)	Base Model
AutoAttack [44]	MIT License	Adversarial Evaluation
LoRA [48]	Apache 2.0	Parameter-efficient Fine-tuning